Available online at www.sciencedirect.com
ScienceDirect
Geochimica et Cosmochimica Acta 70 (2006) 4403–4416
Geochimica
www.elsevier.com/locate/gca

Dissolution kinetics of fosteritic olivine at 90–150 °C including effects of the presence of CO_2

M. Hänchen [a], V. Prigiobbe [a], G. Storti [b], T.M. Seward [c], M. Mazzotti [a,*]

[a] Institute of Process Engineering, ETH Zurich, 8092 Zurich, Switzerland
[b] Institute for Chemical and Bio-Engineering, ETH Zurich, 8092 Zurich, Switzerland
[c] Institute for Mineralogy and Petrology, ETH Zurich, 8092 Zurich, Switzerland

Received 13 January 2006; accepted in revised form 27 June 2006

Abstract

The steady state dissolution rate of San Carlos olivine [$Mg_{1.82}Fe_{0.18}$ SiO_4] in dilute aqueous solutions was measured at 90, 120, and 150 °C and pH ranging from 2 to 12.5. Dissolution experiments were performed in a stirred flow-through reactor, under either a nitrogen or carbon dioxide atmosphere at pressures between 15 and 180 bar. Low pH values were achieved either by adding HCl to the solution or by pressurising the reactor with CO_2, whereas high pH values were achieved by adding LiOH. Dissolution was stoichiometric for almost all experiments except for a brief start-up period. At all three temperatures, the dissolution rate decreases with increasing pH at acidic to neutral conditions with a slope of close to 0.5; by regressing all data for $2 \leqslant \text{pH} \leqslant 8.5$ and $90\ ^\circ\text{C} \leqslant T \leqslant 150\ ^\circ\text{C}$ together, the following correlation for the dissolution rate in CO_2-free solutions is obtained:

$$r = A a_{H^+}^n \exp\left(\frac{-E_a}{RT}\right)$$

with $A = 0.0854$ (+0.67 to −0.076), the activation energy $E_a = 52.9 \pm 6.9$ kJ mol^{-1} K^{-1}, $n = 0.46 \pm 0.03$ ($R^2 = 0.98$) and r in [mol cm^{-2} s^{-1}], based on a 95% confidence interval. Data were fitted to a shrinking particle model, being based on the assumption of surface controlled dissolution throughout the whole experiment, with dissolution extent varying from less than 1% up to complete dissolution, depending on the experimental conditions. In the presence of CO_2 and at low pH, dissolution rates exhibited the same behaviour as a function of pH, however at pH > 5 the rate decreased much more rapidly with pH than in the presence of N_2. The presence of citric acid, an organic ligand, increased dissolution rates in respect to the baseline HCl solution significantly.

1. Introduction

The dissolution and reactivity of silicate minerals on the Earth's surface have proceeded throughout geological time in response to and in concert with changes in atmospheric chemistry and geophysical phenomena as manifested by global tectonics. The interaction of natural waters with silicate minerals plays an important role in the global carbon cycle and, in particular, the release of magnesium and calcium during silicate mineral dissolution comprises an important aspect of the global sequestration of atmospheric CO_2. In addition, magnesium silicate dissolution and hydrolysis equilibria play a fundamental role in defining important aspects of the chemistry of seafloor hydrothermal systems and the alteration of oceanic crust. However, the kinetics of all the relevant heterogeneous mineral equilibria are essentially unknown under hydrothermal conditions.

The aim of this study is to provide kinetic data for the dissolution of olivine at elevated temperature and under high CO_2 pressure and to study effects of solution composition. The dissolution of olivine, and that of other silicates like serpentine, is one of the main rate-limiting steps of mineral carbonation, a novel technology which strives to store anthropogenically generated CO_2 in solid Mg- and

* Corresponding author. Fax: +41 44 632 1141.
E-mail address: marco.mazzotti@ipe.mavt.ethz.ch (M. Mazzotti).

0016-7037/$ - see front matter © 2006 Elsevier Inc. All rights reserved.
doi:10.1016/j.gca.2006.06.1560

Ca-carbonates. It involves the dissolution of Mg- and Ca-rich silicates in aqueous solutions, at high temperatures and under high CO_2 pressure, followed by the precipitation of carbonates. The idea of mineral carbonation was first developed by Lackner et al. (1995) and is part of a portfolio of different carbon dioxide capture and storage (CCS) technologies, intended to reduce human-induced carbon dioxide emissions into the atmosphere (IPCC, 2005).

Dissolution kinetics for olivine and serpentine, the two main source minerals for mineral carbonation, have been studied for several decades; especially, olivine has attracted noticeable interest, mainly due to its structural simplicity and high reactivity (Wogelius and Walther, 1991; Chen and Brantley, 2000; Pokrovsky and Schott, 2000; Rosso and Rimstidt, 2000; Oelkers, 2001). However, almost all studies were conducted at temperatures between 25 and 65 °C and at ambient pressure (see overview by Rosso and Rimstidt, 2000), whereas the optimal reaction temperatures for the process of mineral carbonation have been found to be between 150 and 200 °C and at CO_2 pressures of up to 250 bar (O'Connor et al., 2004). In addition, the presence of CO_2, a major factor in the carbonation results reported so far, has only been looked at in a few cases (Pokrovsky and Schott, 2000). Other factors, like the effect of ligands have only been studied at ambient temperature (Grandstaff, 1986; Wogelius and Walther, 1991).

It has been recognised in the literature that dissolution rates of silicates are typically reproducible to within ±0.25 log units within one laboratory and to within two orders of magnitude among different laboratories, which illustrates the difficulties one faces in comparing reported dissolution rates (Kump et al., 2000). These differences stem both from the varying properties of natural minerals and from experimental difficulties, e.g., very low aqueous concentrations.

In the following, we report dissolution rates of olivine at 90, 120, and 150 °C, the effect of CO_2 and citric acid, and discuss these results in comparison with previous studies.

2. Dissolution of olivine

2.1. General dissolution kinetics

The dissolution rate of olivine exhibits a marked dependence on the solution pH, as it has been noted with other silicate minerals. This dependence represents a trend that is independent of the absolute value of the dissolution rate, and is based upon a quite large dataset. At acid to neutral conditions and ambient temperature, the exponent, n, in the relationship $r \propto a_{H^+}^n$ has been found in many dissolution studies to be close to 0.5 over the range of pH 2–6, with r being the dissolution rate and a_{H^+} the hydrogen ion activity. At basic conditions, the trend is less clear and only few results have been published; however, they indicate that the dissolution rate is no longer a function of pH above pH 7–8. An overview of previous studies of olivine dissolution is given in Table 1, listing the conditions under which experiments were carried out and the reported values for the dissolution rate, pH dependence, and activation energy.

Two different reaction mechanisms have been proposed by Pokrovsky and Schott (2000), a first one governing the dissolution at pH lower than 7, being pH dependent, and a second one becoming dominant at pH higher than 8 and exhibiting no pH dependence. The first mechanism involves the adsorption of one H^+ ion onto two elemental cells of olivine, resulting in the cited pH dependence. This is accompanied by the extraction of Mg^{2+} ions and the formation of a very thin Mg-depleted layer on the surface. The second mechanism is based upon the formation of $MgOH_2^+$ surface groups, which form after the extraction of SiO_2, whose concentration determines the dissolution rate, and whose formation and detachment is independent of pH, thus explaining the independence of the dissolution rate of pH. A thin Si-depleted surface layer is formed under these conditions (Pokrovsky and Schott, 2000). There is no clear agreement about whether the pH dependence changes with increasing temperatures, with two studies reporting no change with temperature, and two others finding values for n between 0.33 and 0.7 at higher temperatures (see Table 1).

Another quantity, the activation energy, is less well estimated, with reported values varying between 25 and 125 kJ/mol. This range can be narrowed, however, as a more detailed discussion will show later.

Under the assumption that the pH dependence is independent of temperature, the following correlation can be used to describe dissolution rates:

$$r = A a_{H^+}^n \exp\left(\frac{-E_a}{RT}\right) \quad (1)$$

with r being the dissolution rate [mol cm^{-2} s^{-1}], A a pre-exponential factor [mol cm^{-2} s^{-1}], E_a the activation energy [kJ mol^{-1}], T the temperature [K], $R = 8.3145$ kJ mol^{-1} K^{-1} the gas constant, a_{H^+} the hydrogen ion activity [−], and n the reaction order with respect to H^+.

If one wants to account for a change in pH dependence with temperature—for which non-consistent results have been reported—it is either necessary to find a correlation for n with temperature, or to calculate a pH-dependent activation energy, leading to the following expression:

$$r = B \exp\left(\frac{-E_a^*}{RT}\right) \quad (2)$$

where B is a pH-dependent pre-exponential factor [mol cm^{-2} s^{-1}], and E_a^* the pH-dependent activation energy. E_a^* for pH 0 is equal to the standard pH-independent activation energy. This approach has only been implemented by Chen and Brantley (2000), combining their own results with those of other groups.

Dissolution rates are usually expressed in moles per unit area per unit time, with the effective surface area being

Table 1
Olivine dissolution results

	Awad et al. (2000)[a]	Blum and Lasaga (1988)	Chen and Brantley (2000)	Grandstaff (1986)[b]	Jonckbloedt (1998)[c]	Oelkers (2001)	Pokrovsky and Schott (2000)	Rosso and Rimstidt (2000)	Van Herk et al. (1989)	Wogelius and Walther (1992)
Temperature	23–90 °C	25 °C	65 °C	1–49 °C	60–90 °C	25–65 °C	25 °C	25–45 °C	40–70 °C	25–65 °C
pH	1, 2	2–5, 9, 11	2–5	2.9–5	–0.7–2	2	1–12	1.8–3.8	1–3	2–12.4
pH dependence (pH ⩽ 6)	0.48/0.40 (50/70–90 °C)	0.56	0.7	1.1 (25 °C)	0.33	—	0.5	0.5	—	0.54
Activation energy [kJ mol^{-1}]	71.5 (±12) (bulk)[d]	—	126 (at pH 0)[e]	38.1 (±1.7)	66.5 (±2)	63.8 (±17)	—	42.6 (±0.8)	55/67 (HCl/H_2SO_4)[f]	79.5 (±10)
Dissolution rate (25 °C, pH 2) [mol cm^{-2} s^{-1}][g]	1.3×10^{-11}	1.1×10^{-12}	—	*1.9×10^{-13}*	*3.9×10^{-11}*	1.3×10^{-12}	2.3×10^{-12}	1.2×10^{-12}	—	7.6×10^{-13}
BET area over geom. area	—	—	1.9 (Kr)	52 (N_2)	—	3.1 (Kr)	3.1 (Kr)	5.7 (N_2)	39 (N_2)	6.2 (Kr)

[a] Measuring the shrinking of small olivine cubes; rates are relative to geometric surface area not BET surface area.
[b] Reporting a much higher BET surface, which, if correct, would indicate bigger internal surfaces, with diffusion limitations possibly causing a different dissolution behaviour.
[c] Rates relative to geometric surface of spherical particles.
[d] 114.5, 69.9 and 72.9 [kJ mol^{-1}] along three different perpendicular axis.
[e] 113/104/92/83 [kJ mol^{-1}] at pH 1/2/3/4, derived by combining their results with those from Blum and Lasaga, 1988; Wogelius and Walther, 1992.
[f] Correcting the omission of the factor ln(10) in their calculations.
[g] Using Eq. (1) with fitted parameters; extrapolated values in italics.

determined by krypton or nitrogen gas adsorption, using the BET method. Already at this stage, differences are introduced since for example using nitrogen usually results in larger surface areas than using krypton (Brantley and Mellott, 2000). Furthermore, small impurities with much higher specific surfaces, such as talc, can introduce significant errors (Brantley and Mellott, 2000). The convention is to express all rates relative to the initial surface area, assuming that for slow dissolution rates the effective surface does not change significantly over the course of the experiment. To compare the measured surface areas reported by the different groups, it is necessary to normalise the area with respect to the particle size distribution of the measured samples. The following ratio can be defined:

$$q_A = \frac{a_{sp}\rho d_M}{6} \tag{3}$$

with a_{sp} being the BET surface area [cm^2 g^{-1}], ρ the density of olivine [g cm^{-3}], and d_M the geometric mean of the particle diameter calculated from the lower and upper limit of the particle size range [cm]. The ratio q_A quantifies the difference between the BET area and the geometric surface of a sphere of the same particle size. Such difference is due to surface roughness, to deviations from the spherical shape and to the physics of the BET surface measurement. Even for a population of particles from the same sieve fraction and with similar surface characteristics, q_A may differ due to differences in the particle size distribution, because of the presence of fines. Calculating this value for a large number of reported BET surface area measurements in the literature, it can be seen that in the majority of cases a value between 2 and 6 is found. The much higher values found by Van Herk et al. (1989) and Grandstaff (1986) indicate either measurement errors or the use of olivine with noticeably higher (internal) surfaces, e.g. in the form of cracks, imperfect removal of fines, or the presence of impurities of other minerals.

Using Eq. (1) with the fitted parameters from five earlier studies, the dissolution rate of olivine at 25 °C and pH 2 is found to vary between 8×10^{-13} and 2.3×10^{-12} mol olivine cm^{-2} s^{-1}, with three of the five values being between 1.1×10^{-12} and 1.3×10^{-12} mol cm^{-2} s^{-1} (see Table 1 for references). Awad et al. (2000), using the completely different experimental approach of measuring the size of small dissolving olivine cubes instead of measuring the release of ions into the solution, reported a noticeably higher value of 1.3×10^{-11} mol cm^{-2} s^{-1}. Since the BET surface area was not determined by them, this number refers to the geometric surface area of their cubic particles instead. At higher pH values, the spread among the reported rates is getting slightly larger but the relative order among the different studies is maintained. Considering also extrapolated values from Rosso and Rimstidt (2000), the reported values at pH 6 and 25 °C vary between 5×10^{-15} and 2.3×10^{-14} mol cm^{-2} s^{-1}, with an unweighted average of 1.2×10^{-14} mol cm^{-2} s^{-1}.

At 45 °C and pH 2, the values from two studies (Rosso and Rimstidt, 2000; Oelkers, 2001), having almost identical rates at 25 °C, differ by a factor of two. At 65 °C and pH = 2, another study (Chen and Brantley, 2000) reported a dissolution rate five times higher than those of Oelkers (2001), which already represented a higher end value at 45 °C. Experimental results at up to 90 °C are available from two studies using different experimental approaches than the previously mentioned studies (Awad et al., 2000; Jonckbloedt, 1998). Although their dissolution rate values cannot directly be compared to other findings since the BET surface area can only be estimated in these cases, the activation energies, obtained at elevated temperatures, can, however, be compared and do not differ significantly from those measured at lower temperature.

In extrapolating these data to 150 °C and above, the choice of activation energy is crucial. Excluding values found by combining the results of different studies (Chen and Brantley, 2000), those using proxy data (Brady et al., 1999), as well as those derived from very small data sets and partly incongruent dissolution (Wogelius and Walther, 1992) and correcting an error in those found by Van Herk et al. (1989), the two lowest values found are 38 and 43 kJ/mol, with the latter being based on the large data set of Rosso and Rimstidt (2000). Four other groups report figures between 55 and 72 kJ/mol with standard deviations between 2 and 17 kJ/mol. Awad et al. (2000) measured different activation energies and dissolution rates along different crystallographic axes, concluding that the bulk activation energy should increase with temperature as dissolution along one axis becomes dominant. Extrapolating the dissolution rates along the three different axis separately by using the respective activation energies and dissolution rates would roughly double the estimated bulk dissolution rate at 150 °C with respect to the conventional approach of scaling the dissolution rate with a constant activation energy. This comparison uses for the latter approach the bulk activation energy calculated by Awad et al. (2000), which is already the highest activation energy reported.

2.2. Effect of ligands

Numerous studies have demonstrated the significant influence of (organic) ligands on dissolution rates of silicates (e.g., Furrer and Stumm, 1986). Wogelius and Walther (1991) showed a marked increase in the dissolution rate of olivine in solutions containing potassium hydrogen phthalate (KHP)–HCl buffer as well as solutions containing ascorbic acid over the range of pH 2–6 compared to HCl solutions, with the effect increasing with pH, thus resulting in a much reduced pH dependence. Following Furrer and Stumm (1986), they argue that the formation of surface complexes, upon the adsorption of organic compounds, creates the precursors, which then detach from the mineral surface. They further theorise that a negatively charged ligand adsorbs on a hydrated Mg surface site $MgOH_2^+$. The levelling-off of the effect of different ligands (KHP, ascorbate) towards lower pH values was conjectured to come from the saturation of the surface sites or the ligands with protons. The dependence on the ligand concentration was found to be very similar to the hydrogen ion dependence, with an exponent of 0.6.

Grandstaff (1986) measured dissolution rates of olivine in a number of different ligands. The enhancement effect on the dissolution rate varied among the different compounds as follows: EDTA $\simeq$ citrate $>$ oxalate $>$ tannic acid $\gg$ succinate $>$ phthalate $>$ acetate $\simeq$ KCl. This corresponds to the order of strength of the cation-organic complex. For EDTA the dissolution rate increased by a factor of 100 at 0.01 M compared to a factor of 10 for phthalate and 1.1 for acetate, all at the same concentration. For the three ligands, EDTA, phthalate and fulvic acid the reaction order was found to be close to 0.5. Measuring at two different pH values, 4.5 and 3.5, they also found the effect to decrease markedly with decreasing pH.

Similar effects were also found for the dissolution of serpentine in the presence of ligands, underlining the general nature of cation-ligand interaction (Park et al., 2003).

3. Experimental set-up and methods

Natural San Carlos gem-quality olivine crystals having an average size of ~0.5 cm were handpicked, crushed, and sieved into different size fractions. The size fraction between 90 and 180 μm was cleaned ultrasonically using ethanol to remove adhering fines and dried overnight at 60 °C. The specific surface was measured by nitrogen adsorption using the BET method. The resulting value of $797 \pm 55\ cm^2\ g^{-1}$, corresponds to a ratio q_A of 5.5 (see Eq. (3)). The average composition as measured by electron microprobe analysis was found to be $Mg_{1.82}Fe_{0.18}SiO_4$ ($M_{mol} = 146.4\ g\ mol^{-1}$). The dissolution experiments were performed in a stirred 300 ml titanium (grade 2) flow-through reactor fed by an HPLC pump (see Fig. 1). Agitation was supplied by a blade stirrer suspended from the top of the reactor and driven by a magnetic coupling. In the experiments under a CO_2 atmosphere, a stirrer entraining the gas into the solution was employed to facilitate gas–liquid equilibrium. To ensure that mass transport limitations did not influence the dissolution rate, the effect of the stirring rate was studied at a high dissolution rate, i.e., at the lowest pH value, and the stirrer rate for all experiments was set at a value above which no influence of the stirring rate could be detected under those conditions. The reactor was operated with a liquid volume of between 160 and 180 ml, the remaining volume containing the gas atmosphere. The vessel was held under a nitrogen (grade 5.0, i.e., 99.999% pure) or a carbon dioxide (grade 4.5, i.e., 99.995% pure) atmosphere, with the feed solution being purged of oxygen and other atmospheric components with the same nitrogen. The CO_2 was fed from a high-pressure buffer tank, the N_2 directly from a gas cylinder, both via front pressure regula-

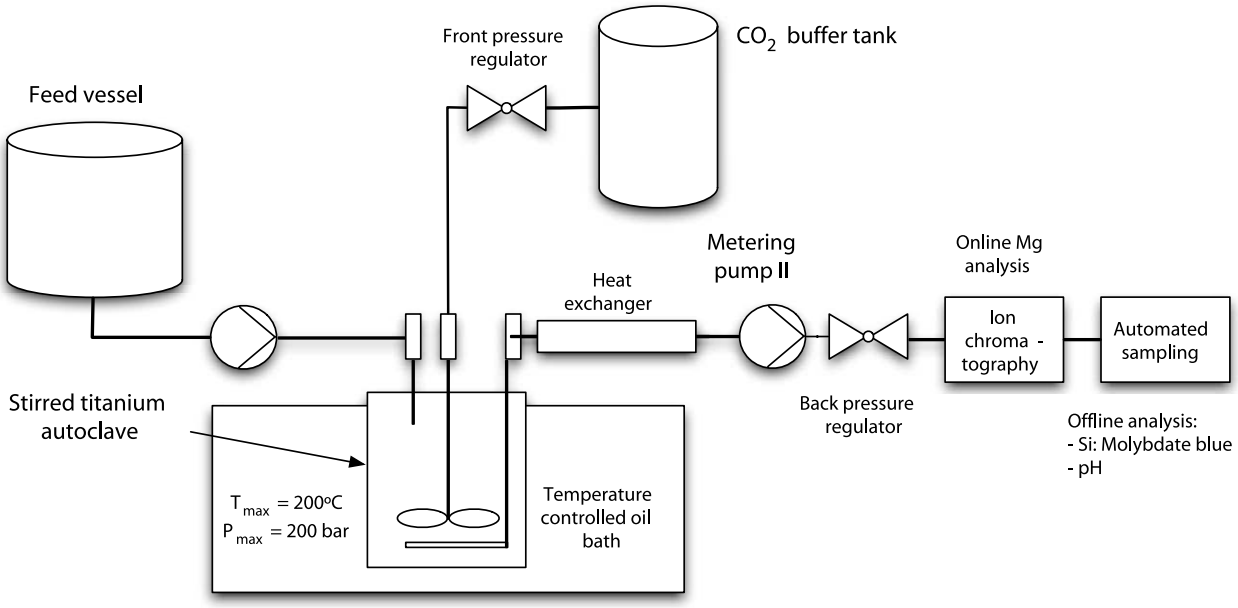

Fig. 1. Scheme of the experimental set-up used for the experiments.

tors. The feed, consisting of distilled water with the pH set by adding HCl or LiOH, was introduced at a constant rate varying between 2 and 10 ml/min. A second HPLC pump was used to withdraw liquid at exactly the same flow rate to maintain a constant liquid level in the reactor. Before passing through the second pump, the outlet stream was cooled down to ambient temperature in a heat exchanger. A backpressure regulator was used to depressurize the effluent to ambient pressure. Samples were taken with a fraction collector at regular intervals; the magnesium concentration in the outlet solution was measured in-line by means of an ion chromatograph (CS12A column, Dionex) and the silica concentration was measured spectrophotometrically using the Molybdate Blue method (Grasshoff and Anderson, 1999, p. 192). For all experiments under a nitrogen atmosphere, the pH was measured with a pH-probe off-line at ambient temperature. To estimate the pH at the experimental temperature, the simulation package EQ3/6 Wolery (1992) was utilized. A database employing an extended Debye–Hückel equation for the estimation of the aqueous activity coefficients was used with it. The fugacity of CO_2, needed as an input parameter for EQ3/6, was calculated with the correlation presented by Wolf et al. (2004). Based on the measured pH and measured magnesium and silica concentration, the actual pH was calculated. Experiments were carried out at 90, 120, and 150 °C, and at pH values between 2 and 12.5.

In the experiments under a N_2 atmosphere, pressure was 50 bar at 90 °C and 20 bar at 120 and 150 °C. For the experiments carried out under a CO_2 atmosphere, no pH measurements were carried out and the pH was estimated based on temperature, CO_2 pressure and cation concentrations. The pH was varied by changing the CO_2 pressure between 15 and 180 bar, and by adding LiOH for the experiments at higher pH; otherwise distilled H_2O only was used.

4. Modelling and analysis of the experimental measurements

Due to the time needed for filling and heating up the reactor, the temperature was not constant during the first 25 min of each experiment, approximately. No data were collected during this start-up period. The first sample was taken directly after the unit was switched to continuous mode, which marked time zero of the experiment, and the measured concentration, $c_{m,o} = c_m(t = 0)$, of this sample was taken as initial condition.

For practical purposes, all experimental concentrations are reported in olivine equivalents, taken as average of the measured magnesium and silica concentrations, $c_{m,Mg}$ and $c_{m,Si}$ [mol l^{-1}], assuming dissolution close to stoichiometric conditions:

$$c_m = 0.5\left(c_{m,Si} + \frac{c_{m,Mg}}{1.82}\right). \quad (4)$$

In the results shown in Figs. 2–5, the aqueous concentrations in olivine equivalents of both the experimental values and the model results (explained below), as calculated using Eq. (4), are plotted over time. Fig. 5 illustrates this procedure.

For modelling purposes, a perfectly stoichiometric dissolution can be assumed and c [mol l^{-1}], the metal ion concentration in olivine equivalents, can be defined as follows:

$$c = c_{Si} = \frac{c_{Mg}}{1.82}. \quad (5)$$

As shown in the literature (Oelkers, 2001), the dissolution rate of olivine in highly undersaturated solutions does not depend on the concentrations of the ions released by

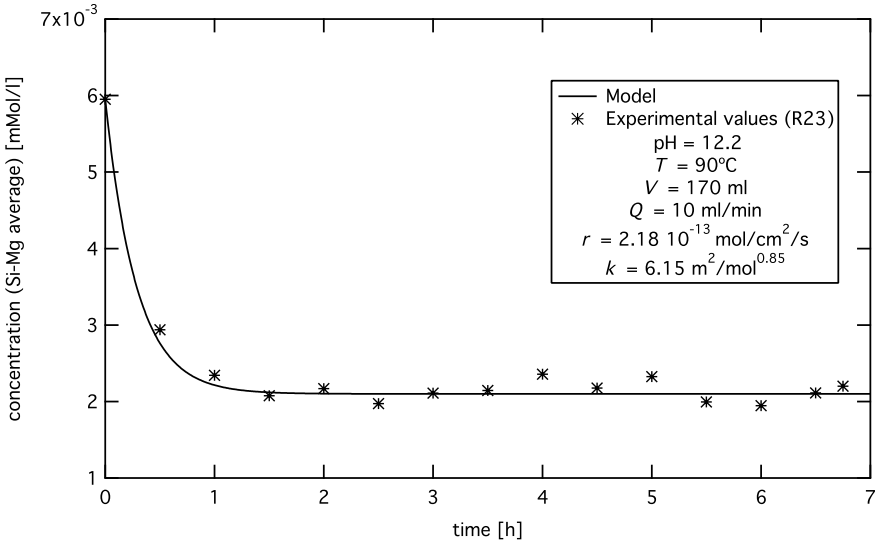

Fig. 2. Slow dissolution at 90 °C: concentration of metal ions, averaged according to Eq. (4), over time for high pH (12.2) experiment, solid line represents modelled concentration.

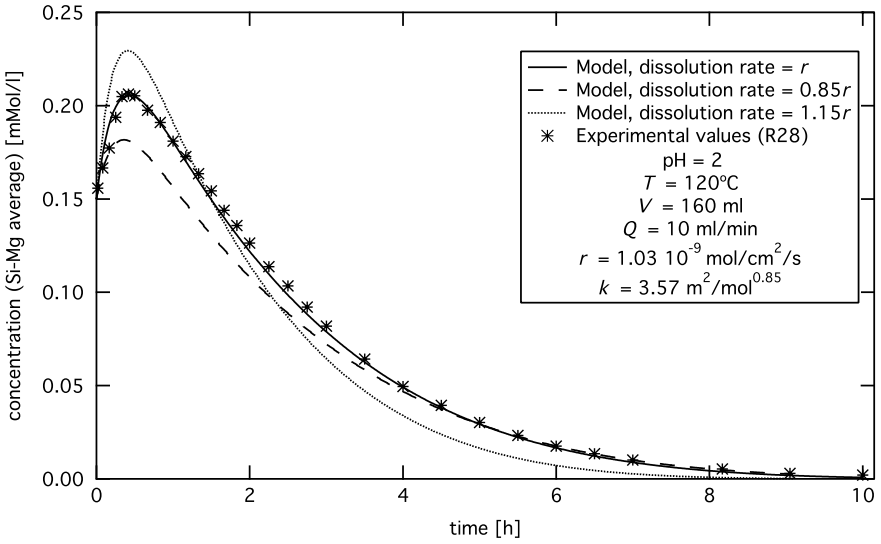

Fig. 3. Fast dissolution at 120 °C: concentration of metal ions, averaged according to Eq. (4), over time for low pH (2) experiment, solid line represents modelled concentration, dashed and dotted lines represent modelled concentrations using dissolution rates reduced or increased by 15% in respect to solid line.

the dissolving mineral but is proportional to the surface area. With saturation indices below −2, this situation certainly applies to our experiments; the saturation index SI is the (decimal) logarithm of the ratio of the activity product over K_{sp}:

$$SI = \log \frac{\prod_i a_i^{\nu}}{K_{sp}} \tag{6}$$

with a_i being the activity of the aqueous ions [–], ν the stoichiometric coefficient [–] and K_{sp} the solubility product [–].

Low temperature dissolution experiments of sparingly soluble material are usually assessed by expressing the dissolution rate with respect to the initial BET surface area. This, however, becomes impractical when during the course of the experiment more than a few percent of solid material are dissolved. Under these conditions, the total available surface area, A_{tot}, is reduced as the particles decrease in size.

Deriving the dissolution rate per unit surface area from measured concentration values and using the BET surface as reference, therefore, requires a model that describes how two quantities that change significantly during the course of an experiment vary, i.e., the metal ion concentration c and the total available surface. To that effect, the two following mass balances, one over the metal ions in the liquid phase and one over the metal ions in the solid phase, i.e., the mineral, have to be considered:

$$V \frac{dc}{dt} = -Qc + R \tag{7}$$

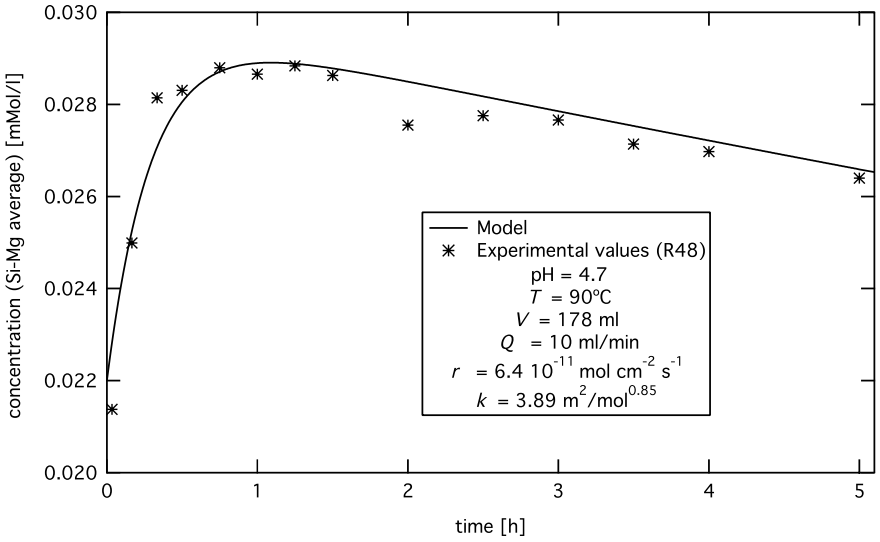

Fig. 4. Dissolution at 90 °C in the presence of citric acid: concentration of metal ions, averaged according to Eq. (4), over time, citric acid concentration 10^{-4} M, pH 4.7, solid line represents modelled concentration.

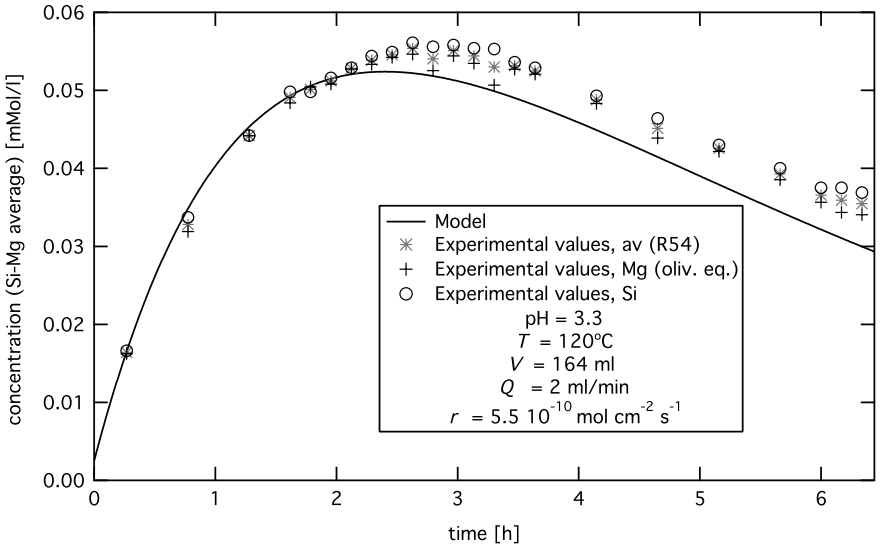

Fig. 5. Dissolution at 120 °C in the presence of CO_2: concentration of metal ions over time, * averaged data according to Eq. (4); +, Mg concentration in olivine equivalents (cf. Eq. (5)), ○, Si concentration, $p(CO_2) = 100$ bar, solid line represents modelled concentration.

$$\frac{dm}{dt} = -R \tag{8}$$

with V [l] being the liquid volume in the reactor, Q [l s^{-1}] the flow rate of the stream leaving the reactor, R [mol olivine s^{-1}] the absolute dissolution rate, m [mol olivine] the amount of the solid in the reactor.

Eqs. (7) and (8) are to be solved by a constitutive equation providing an expression for the absolute dissolution rate R in terms of the unknowns c and m. Such constitutive equation is defined based on the assumptions that characterise the dissolution model adopted in this work.

The first assumption is that the specific dissolution rate r [mol cm^{-2} s^{-1}] given by

$$R = rA_{tot} \tag{9}$$

is constant throughout the whole experiment, with A_{tot} [cm^2] being the total available surface area.

As a second assumption, a general approach to relate the total surface area of dissolving particles to their volume or their mass is used. It assumes that A_{tot} is proportional to m^p (Jonckbloedt, 1998). For mono-sized convex particles with constant shape factors $p = \frac{2}{3}$, for particle size distributions $p \geqslant 0.67$, its actual value depending on the shape of the distribution. Therefore, R can be expressed as

$$R = rkm^p \tag{10}$$

with k [cm^2 mol^{-p}] being a proportionality factor. As a last step, the initial total available surface area is set equal to the area determined by the BET area measurement:

$$A_{tot,i} = a_{sp,i}m_i = km_i^p \tag{11}$$

$$k = a_{\mathrm{sp,i}} m_{\mathrm{i}}^{1-p} \tag{12}$$

with $a_{\mathrm{sp,i}}$ [cm^2 mol^{-1}], and the initial amount, m_{i}. This approach ensures consistency with literature data being based on the initial BET surface area.

Initial values for the integration of this model are $c_{\mathrm{m,o}}$, as defined earlier, and the amount of solid at time zero, m_o:

$$m_{\mathrm{o}} = m_{\mathrm{i}} - V c_{\mathrm{m,o}}. \tag{13}$$

The particle dissolution model shows how the specific surface varies during the dissolution. This is defined by $A_{\mathrm{tot}/m}$, which using Eqs. (9) and (10) can be written as:

$$\frac{A_{\mathrm{tot}}}{m} = \frac{k}{m^{1-p}}. \tag{14}$$

Since $p < 1$ (see below), the specific surface, as described by our model, increases with time as m decreases, i.e. as dissolution proceeds. If this specific surface is interpreted as the BET surface of the dissolving particles, then this observation indicates that our model is consistent with the experimental evidence that BET surface increases during dissolution (Chen and Brantley, 2000; Gautier et al., 2001).

Numerical integration of these equations yields $c = c(t)$, $m = m(t)$, where $c(t)$ can be compared with the experimental evolution of the concentration plotted in Figs. 2–5. Integration depends on p and r; choosing different values leads to different concentration profiles. Since p only accounts for the shrinking of particles, it is therefore only a function of the particle size distribution. Hence, with all olivine coming from the same batch, p can be considered as constant for all experiments. A value of $p = 0.85$ provided the best fit for the ensemble of all experiments and was therefore used. The specific dissolution rate, r, is of course the quantity we want to obtain, hence it changes from experiment to experiment. In Fig. 3, the modelled concentration for three different dissolution rates is shown. By choosing the dissolution rate whose corresponding concentration profile is the closest fit to the experimental data, the actual value of r for each experiment is determined.

Two examples of dissolution under a nitrogen atmosphere without additives are presented, a slow dissolution experiment at 90 °C and high pH (Fig. 2) and a fast dissolution experiment at 120 °C and low pH (Fig. 3). In the case of fast dissolution, the concentration increases initially, as the influx of ions from dissolution into the liquid phase in the reactor surpasses its removal by the outgoing liquid stream. After reaching a peak, the concentration falls again as the particles decrease in size, and as a consequence their surface area as well, and the absolute dissolution decreases. With the particles dissolving almost completely towards the end, the concentration in the reactor approaches asymptotically zero.

Two further examples, in the presence of citric acid (Fig. 4) and under a CO_2 atmosphere (Fig. 5), follow the same pattern, albeit with slower dissolution rates, and for the experiment with CO_2 with a much longer start-up phase due to a lower flow rate through the reactor. This shows that the presence of CO_2 and citric acid does not alter the underlying principle of surface controlled dissolution.

This notwithstanding, a simplified approach could be taken for high pH experiments where dissolution rates are too slow to lead to any noticeable change in the surface area over the course of the experiment. After a start-up period, a steady state is reached under these conditions, where a simple mass balance of the liquid phase in the reactor, in other words the steady state solution of Eq. (7), yields an explicit equation for the dissolution rate, as it has been applied for low-temperature experiments in the literature:

$$r = \frac{Q c_{\mathrm{m}}}{a_{\mathrm{sp}} m}. \tag{15}$$

The time needed to reach the steady state is determined by the average residence time of the aqueous solution in the reactor, i.e., the ratio between the reactor volume and the flow rate, lasting between one and 6 h in our experiments depending on the respective flow rate through the reactor. The achievement of a steady state after a little more than one hour can clearly be seen in Fig. 2.

5. Results and discussion

5.1. Experiments without CO_2

The reaction rates, measured and regressed as described above, are reported in Table 2 and shown in Fig. 6 as function of the pH at experimental conditions for 90, 120, and 150 °C together with data reported in the literature at 25 °C (Pokrovsky and Schott, 2000). In addition to the dissolution rate obtained as described in the previous section, the table lists the operating parameters temperature, flow rate and amount of olivine and the aqueous concentration in olivine equivalents (i.e., Aq. conc. in Tables 2–4). This latter is calculated by taking an average of the magnesium and silica values for each sample as described by Eq. (4) and calculating the average over the whole experiment duration. The pH at high temperature is calculated using this average concentration. Furthermore, the experiment duration, the amount dissolved and the Mg/Si ratio are shown. The same values and additionally the CO_2 pressure and the lithium or citric acid concentrations are shown in Tables 3 and 4.

The dependence of the dissolution rate on pH follows a trend found already at lower temperature. Up to about pH 8, the logarithm of the rate can be regressed linearly. For pH values higher than that, the dissolution rate only shows a very weak dependence on pH, confirming the trend found at lower temperature. Regressing all data up to pH 8.5 together, yields the correlation listed below:

$$r = A a_{\mathrm{H^+}}^{n} \exp\left(\frac{-E_{\mathrm{a}}}{RT}\right)$$

with $A = 0.0854$ (+0.67 to −0.076), the activation energy $E_{\mathrm{a}} = 52.9 \pm 6.9$ kJ mol^{-1} K^{-1}, $n = 0.46 \pm 0.03$ ($R^2 = 0.98$)

Table 2
Operating conditions and experimental results of experiments under nitrogen atmosphere (see text for explanation of values)

T [°C]	pH at 25 °C	pH at high temp.	$-\log r$	r [mol cm^{-2} s^{-1}]	Aq. conc. [μM]	Flow rate [ml min^{-1}]	Amount olivine [mg]	Fraction dissolved [−]	Duration [h]	Mg/Si ratio [−]	Exp. No.
90	2.01	2.01	9.658	2.20E−10	169.8	10	283.0	0.706	11.8	1.89	R12
90	2.02	2.03	9.658	2.20E−10	166.7	10	286.0	0.697	11.5	1.89	R11
90	3.02	3.02	10.06	8.70E−11	88.2	10	256.4	0.321	10	1.85	R15
90	3.66	3.66	10.102	7.90E−11	59.1	10	200.0	0.356	12.5	1.86	R17
90	4.58	4.59	10.767	1.71E−11	20.0	10	258.9	0.088	12.5	1.83	R14
90	5.25	5.33	11.225	5.95E−12	8.5	10	305.6	0.030	11.8	1.65	R18
90	5.67	6.19	11.79	1.62E−12	15.8	10	2016.7	0.008	11	1.72	R22
90	6.45	7.62	12.133	7.36E−13	7.1	10	1990.0	0.003	9.8	1.97	R21
90	6.64	7.84	12.03	9.33E−13	8.4	10	1990.0	0.006	15	2.21	R20
90	10.18	11.94	12.983	1.04E−13	5.5	2	2008.0	0.001	14	1.92	R24
90	10.37	12.21	12.662	2.18E−13	2.1	10	2016.0	0.001	6.8	1.39	R23
120	2.02	2.01	8.987	1.03E−09	101.2	10	54.0	0.999	10	1.70	R28
120	2.00	2.02	8.951	1.12E−09	61.7	10	59.0	0.999	9.5	1.59	R27
120	2.01	2.02	8.886	1.30E−09	130.8	10	58.8	0.998	7	1.82	R34
120	4.17	4.24	10.036	9.20E−11	60.4	10	149.0	0.116	3	1.74	R37
120	5.14	5.13	10.398	4.00E−11	76.1	5	203.2	0.089	5	1.83	R36
120	5.37	6.31	10.914	1.22E−11	23.9	10	400.5	0.023	4	1.80	R29
120	5.48	6.49	10.884	1.31E−11	23.3	10	400.9	0.023	4	1.85	R30
120	7.59	8.33	11.796	1.60E−12	13.2	5	1001.7	0.007	10	2.10	R32
120	8.69	9.44	11.678	2.10E−12	15.3	5	798.6	0.014	15.6	2.20	R33
120	10.59	12.54	12.5	3.16E−13	1.8	4	741.7	0.001	5	0.76	R39
150	2.02	2.03	8.425	3.76E−09	135.9	10	99.8	1.000	9.2	1.74	R41
150	2.92	2.93	8.783	1.65E−09	60.2	10	31.6	1.000	6.7	1.90	R50
150	3.79	3.82	9.542	2.87E−10	62.9	10	60.1	0.619	7.2	1.82	R58
150	4.53	4.76	9.77	1.70E−10	72.1	10	102.6	0.267	4.1	1.83	R40
150	5.13	5.64	10.201	6.30E−11	28.6	10	100.9	0.106	4	1.89	R43
150	5.17	5.72	10.187	6.50E−11	28.3	10	100.2	0.184	7	1.88	R42
150	6.32	6.75	10.939	1.15E−11	5.6	10	99.8	0.039	8	2.53	R44
150	6.90	7.34	10.824	1.50E−11	17.4	4	100.1	0.052	7.9	2.50	R45

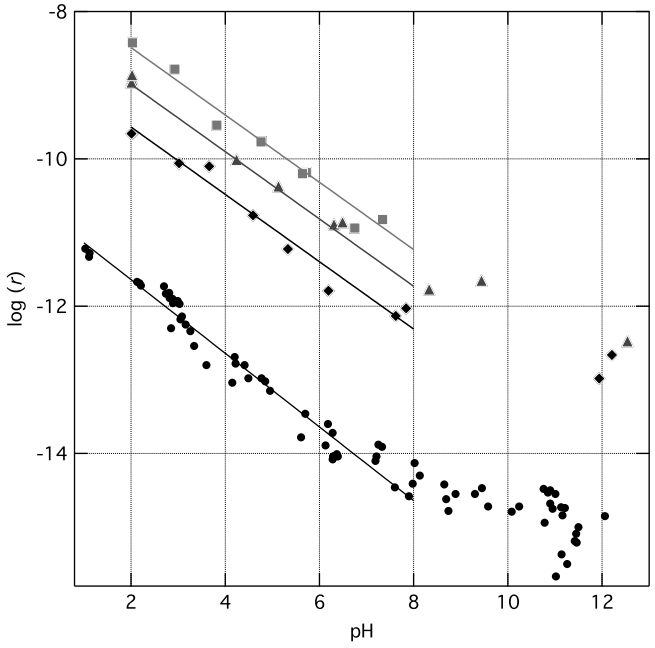

Fig. 6. Dissolution rate of olivine, r [mol cm^{-2} s^{-1}], vs. pH ● at 25 °C taken from Pokrovsky and Schott (2000), ♦ our data at 90 °C, ▲ at 120 °C and ■ at 150 °C (Si–Mg average), lines depict correlations for the four temperatures.

and r in [mol cm^{-2} s^{-1}], based on a 95% confidence interval.

The value for the coefficient n, describing the pH dependence, is within the range of those reported in the literature at lower temperature, and close to its theoretical value of $n = 0.5$. Regressing the data for each temperature individually results in slightly varying coefficients, namely $n = 0.45$, 0.45, and 0.48 at 90, 120, and 150 °C, respectively. As in most earlier studies, n does not appear to change significantly with temperature. Moreover, extrapolations based on the theoretical value of $n = 0.5$ and the average dissolution rate found at pH 2 and 25 °C scaled with the upper end of the range for the activation energy of 70 kJ/mol to a temperature of 90 °C give a rate of 1.9×10^{-10} at pH 2 and 1.9×10^{-12} mol cm^{-2} s^{-1} at pH 6. The corresponding values derived from our data, 2.7×10^{-10} and 4.0×10^{-12} mol cm^{-2} s^{-1}, are in a remarkably good agreement with these predictions.

The activation energy for the regression of all data is $E_a = 52.9$ kJ mol^{-1}. Considering only the data at 90 and 120 °C together, an activation energy of $E_a = 60.2$ kJ mol^{-1} is found, and using only results at 120 and 150 °C an activation energy of $E_a = 43.9$ kJ mol^{-1}. All values are within the range of those reported previously

Table 3
Operating conditions and experimental results of experiments under CO_2 atmosphere (see Section 5.1 for explanation of values)

T [°C]	$p(CO_2)$ [bar]	c(Li) [mM]	pH	$-\log r$	r [mol cm^{-2} s^{-1}]	Aq. conc. [μM]	Flow rate [ml min^{-1}]	Amount olivine [mg]	Fraction dissolved [−]	Duration [h]	Mg/Si ratio [−]	Exp. No.
90	180	0	3.18	9.824	1.50E−10	53.01	2	15.5	0.382	4.5	1.72	R53
90	140	0	3.25	9.839	1.40E−10	84.42	2	31.2	0.444	7.9	2.05	R52
90	100	0	3.27	9.796	1.60E−10	94.99	2	40.0	0.423	7.7	1.39	R51
120	140	0	3.34	9.149	7.10E−10	61.88	2	6.6	0.660	3.1	2.01	R55
120	180	0	3.29	9.071	8.50E−10	55.06	2	6.1	0.958	6.6	1.61	R56
120	100	0	3.39	9.260	5.50E−10	48.63	2	6.4	0.810	6.3	1.76	R54
120	100	0	3.66	9.409	3.90E−10	303.33	5	100.2	0.502	3.5	1.84	R62
120	15	0	3.84	9.538	2.90E−10	41.92	5	27.7	0.548	5.7	1.97	R64
120	100	40	4.20	9.658	2.20E−10	40.24	2	13.3	0.516	7.4	1.84	R60
120	15	53	5.03	10.222	6.00E−11	36.83	5	68.8	0.223	6.8	2.63	R66
120	15	260	5.69	10.699	2.00E−11	45.02	5	187.0	0.094	11.7	1.90	R68
120	15	591	6.03	11.824	1.50E−12	0.16	5	8.2	0.009	6	n.a.	R61
120	15	600	6.03	11.959	1.10E−12	2.15	4	215.4	0.002	3	n.a.	R65
150	100	0	3.34	8.939	1.15E−09	28.84	2	3.5	0.993	7	1.66	R57
150	140	0	3.39	9.000	1.00E−09	42.13	2	4.7	0.970	6.3	1.90	R59

Table 4
Operating conditions and experimental results of experiments with citric acid under nitrogen atmosphere (see Section 5.1 for explanation of values)

T [°C]	pH at 25 °C	$-\log r$	r [mol cm^{-2} s^{-1}]	Citric ac. conc. [M]	Aq. conc. [μM]	Flow rate [ml min^{-1}]	Amount olivine [mg]	Fraction dissolved [−]	Duration [h]	Mg/Si ratio [−]	Exp. No.
90	3.42	9.959	1.10E−10	1.0E-3	48.8	10	99.6	0.161	3.5	3.798	R46
90	4.53	10.194	6.40E−11	1.0E-4	27.8	10	97.5	0.132	5	1.894	R48

(see Section 2.1). The decrease in the activation energy at higher temperature could be due to inhibiting effects like the formation of iron oxide layers on the surface of the olivine particles, whose extent might increase with increasing temperature. Almost all solutions were supersaturated in respect to several Fe compounds, precipitation of Fe-containing solids cannot be excluded. Measurement of iron concentrations in the effluent, carried out for several 90 °C experiments, exhibited stoichiometric values, thus indicating no significant precipitation of iron in the reactor at this temperature despite the solutions being supersaturated. At all temperatures, no iron-oxide layer formation on the recovered olivine could be detected visually.

Dissolution was stoichiometric throughout almost all experiments, within experimental uncertainty, except for a start-up period observed in the experiments under neutral to alkaline conditions and two experiments at high pH. In these cases, an initial preferential release of silica was

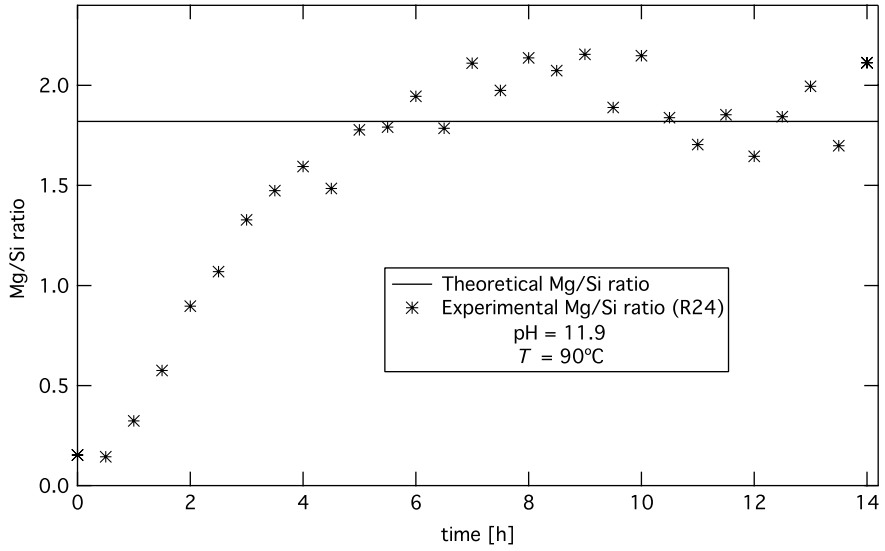

Fig. 7. Magnesium–silica ratio for an experiment at alkaline conditions (pH 11.9, 90 °C) showing an initial preferential release of silica. The horizontal solid line represents the theoretical ratio assuming perfectly stoichiometric dissolution.

recorded (see Fig. 7), in accordance with earlier literature data (Pokrovsky and Schott, 2000). The duration of this start-up phase can be correlated to the dissolution rate itself, in that approximately 0.05% of the solid mass dissolves at neutral to alkaline pH before the Mg/Si ratio approaches stoichiometry. For experiments in the acidic region more than 0.05% of the solid had been dissolved already when the first sample was taken after the start-up time of about 25 min, as mentioned in Section 4, making it impossible to verify the validity of this value in this region. For the two experiments at pH > 12, stoichiometric dissolution was not achieved with the Mg/Si ratio only rising up to 0.8 and 1.4, respectively. In those two experiments only, solutions were supersaturated with respect to brucite, precipitation of which could explain the low Mg/Si ratio. It should be noted that these experiments were not included in the correlation for the dissolution rate, as they are well above pH 8.5 (see above).

5.2. Experiments in the presence of CO_2

In all experiments carried out under a CO_2 atmosphere, ion concentrations were well below the solubility limit of $MgCO_3$ with saturation indices below −2, thus precluding the possibility of $MgCO_3$ precipitation. All results are reported in Table 3. For two experiments, the overall concentrations were so low that the Si concentration was below the determination limit, and therefore, no Mg/Si ratio could be calculated. In the first set of experiments with low Mg-concentrations and no additional alkalinity (Fig. 8), the dissolution rate increases moderately with CO_2 pressure as the pH decreases correspondingly. In the second set, at both 15 and 100 bar of CO_2 pressure, the dissolution rate decreases as the alkalinity, and consequently the pH, is increased by the addition of LiOH or by higher Mg-concentrations. It can be readily observed (Fig. 9) that in the presence of CO_2 and at low pH, dissolution rates exhibited a very similar behaviour as a function of pH as in the experiments without CO_2. However at pH > 5 the rate significantly deviates from its behaviour relative to pH and decreases much more strongly with increasing pH than for CO_2-free solutions. Moreover, the dissolution rate at pH ⩽ 5 in the presence of CO_2 is approximately twice as large as under a nitrogen atmosphere. It should be noted that the three experiments at 90 °C and the two experiments at 150 °C carried out under a CO_2 atmosphere also show higher dissolution rates than the values obtained using the correlation for the experiments under a nitrogen atmosphere.

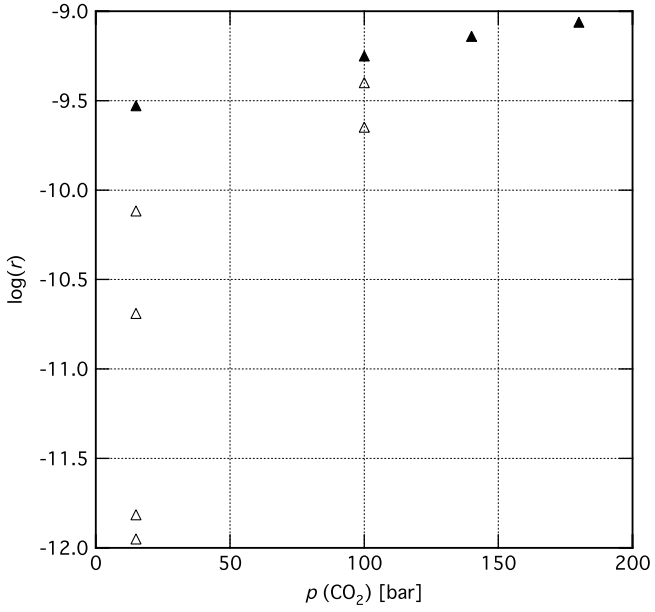

Fig. 8. Dissolution rate of olivine, r [mol cm^{-2} s^{-1}], vs. $p(CO_2)$ at 120 °C: ▲ experiments with low Mg-concentrations and no additional alkalinity, △ experiments with addition of LiOH or increased Mg-concentration.

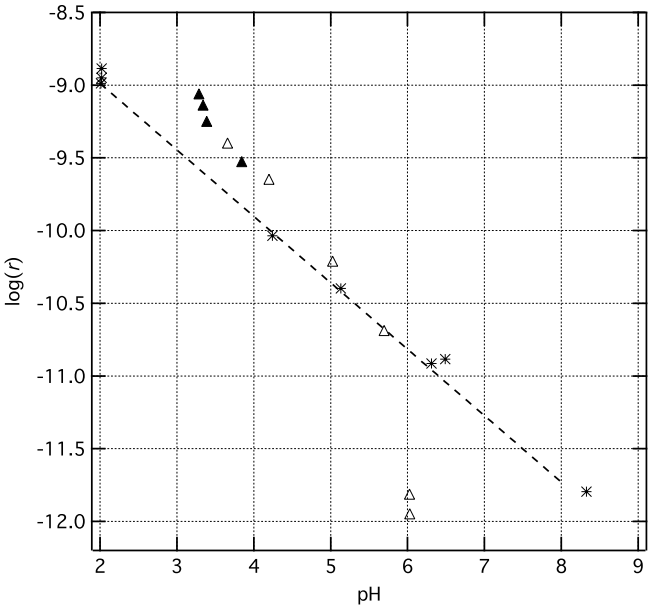

Fig. 9. Dissolution rate of olivine, r [mol cm^{-2} s^{-1}], vs. pH at 120 °C, dashed line is our correlation without CO_2, ∗ experiments without CO_2, ▲ and △ experiments with CO_2.

The drop in the dissolution rates at pH > 5 can be explained by a mechanism suggested by Pokrovsky and Schott (2000) (see Section 2.1). Their proposed mechanism for the dissolution at alkaline conditions involved the formation of $>MgOH_2^+$ surface groups, whose concentration determined the dissolution rate, and whose formation and detachment was independent of pH, thus explaining the independence of the dissolution rate of pH. In the presence of CO_3^- ions, whose concentration increases with increasing pH, these groups could react and form $>MgCO_3^-$ surface groups, thereby inhibiting the dissolution process. The same inhibition mechanism had already been proposed by Wogelius and Walther (1991).

Olivine dissolution results by Pokrovsky and Schott (2000) at low pH and low CO_2 pressure (i.e., at low CO_3^{2-} ion concentration, $m_{CO_3^{2-}} < 10^{-7}$, show dissolution rates that do not differ from those from the correlation

found for CO_2-free solutions. Dissolution was stoichiometric for these cases. Results of Wogelius and Walther (1991) at elevated pH and low CO_2 pressure, having a CO_3^{2-} ion concentration of more than 10^{-4}, show a decrease of the dissolution rate in the presence of CO_2. Experiments under similar conditions by Pokrovsky and Schott (2000) and Golubev et al., 2005 show no decrease with respect to the correlations found by the same authors in CO_2-free solutions. In all three studies, dissolution became increasingly non-stoichiometric with increasing pH, exhibiting an excess of silica.

At low pH ($pH \leqslant 5$) and low CO_3^{2-} concentration ($m_{CO_3^{2-}} < 10^{-7}$), our results agree with literature results in that the presence of CO_2 does not negatively affect the dissolution rate, but rather favours it. At higher pH ($pH > 5$) and higher CO_3^{2-} concentration ($m_{CO_3^{2-}} > 10^{-7}$), comparisons with earlier results are difficult since, as mentioned, there is no agreement with respect to the effect of CO_2 and most reported experiments only exhibited non-stoichiometric dissolution.

The negative deviation of the dissolution rate from its trend in CO_2-free solutions in our results occurs already at a pH between 5 and 6 indicates that at high CO_2 pressure and therefore increased CO_3^{2-} ion concentration (compared to low pressure experiments) this inhibition effect can already become significant under conditions where the surface of the olivine is depleted in magnesium and the dissolution mechanism is not relying on the formation of $> MgOH_2^+$ surface groups.

5.3. Effect of citric acid

As it was described in Section 2.2, organic ligands can enhance dissolution significantly. From the literature, citric acid was found to be one of the most effective compounds. Our experiments with citric acid, conducted at 90 °C, showed that for two out of three experiments (one not shown here) stoichiometric dissolution and could be fitted to a shrinking particle model (see Fig. 4).

In our configuration pH and citric acid concentration were not set independently since citric acid was used to generate acidity. The two experiments reported in Table 4 and shown in Fig. 10 as function of pH were conducted at citric acid concentrations of 10^{-3} M and 10^{-4} M for pH 3.4 and pH 4.5, respectively. The pH values reported here are those measured at ambient temperature since the simulation package EQ3/6 cannot be used for solutions containing citric acid. Correspondingly, the correlation drawn in Fig. 10 was calculated based on the pH measured at ambient conditions. Our results seem to confirm earlier findings (Wogelius and Walther, 1991), with the enhancement effect being more pronounced at higher pH.

6. Experimental and computational uncertainties

Estimating the overall uncertainty from the residuals between our correlation and the measured data yields an error of ±0.020 log units for log r. The overall uncer-

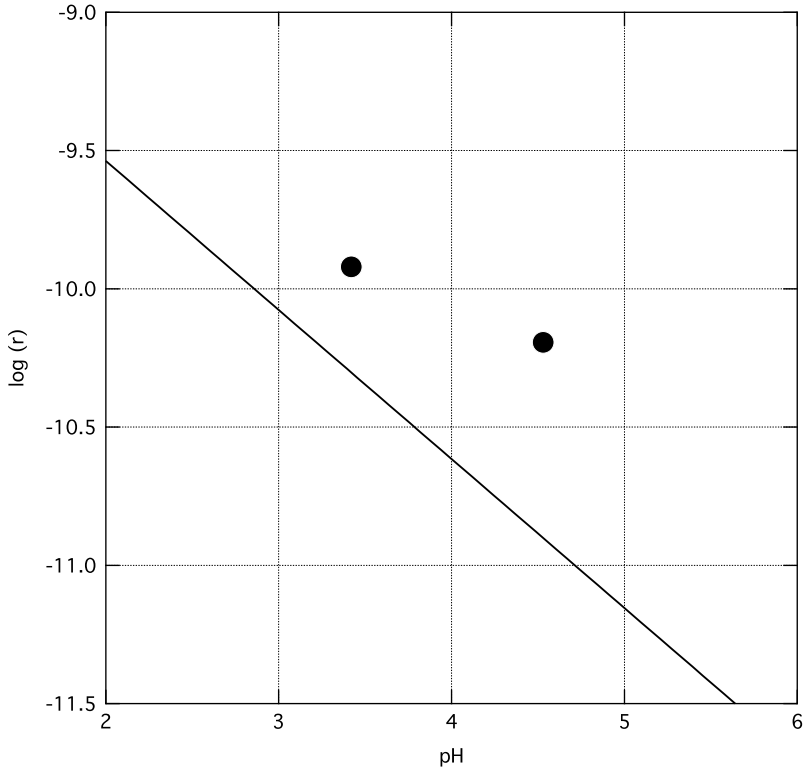

Fig. 10. Dissolution rate of olivine, r [mol cm^{-2} s^{-1}], vs. pH, solid line correlation at 90 °C with HCl, ● experiments at 90 °C with citric acid, pH set by citric acid, citric acid concentration 10^{-3} M and 10^{-4} M for pH 3.4 and 4.5 experiments, respectively (Si–Mg average).

tainty of the dissolution rate stems from errors in four measured quantities, i.e., the aqueous concentrations, the liquid flow rates, the surface area and the mass of the solid. The uncertainties in the measured concentration values can be estimated by calculating the standard deviation of the Mg/Si ratio over all experiments except those where the deviation of the ratio is due to non-random causes, i.e., those at pH > 12. This assumes that the observed deviation of the Mg/Si ratio is only due to uncertainties in the Mg and Si concentration measurements. The standard deviation for the averaged concentration (i.e. Eq. (4)) is thus found to be 12.5%. Uncertainties in the liquid flow rates are less than 1%. The uncertainty for our BET surface area measurement is, as reported in Section 3, less than 7%. The mass of olivine was determined with an uncertainty of less than 1%. Combining these results gives rises to a combined error for the dissolution rate, r, of about 15%. The calculation of the pH is based on measured concentrations as well as measured $p(CO_2)$, measured temperature and measured pH. However, with the calculation being highly non-linear, the error in the calculated pH varies considerably with pH. It ranges from less than 0.01 pH units at pH 2 to about 0.2 pH units close to neutral, and slightly higher at highly alkaline conditions, due to the uncertainty of the concentration of CO_2 present as impurity in the nitrogen used.

7. Conclusions

Our results show that the characterization of the dissolution rate of olivine at low temperature can be extended to higher temperature, including its behavior as a function of pH, and is also valid in cases of almost complete dissolution of the particles. A shrinking particle model, being based on the assumption of surface controlled dissolution, was able to describe dissolution in all experiments, namely those without and with CO_2 and those with citric acid. It should be noted that as p was determined empirically, it might mask additional secondary effects influencing the development of the effective available surface area. The fact that a single value can be applied to a wide variety of operating conditions shows that these secondary effects can only have a small influence on the actual effective available surface area. In the presence of CO_2, and at pH $\leqslant$ 5 (at 120 °C), dissolution rates are two times larger than those without CO_2 at the same pH. Citric acid, as other ligands previously studied in the literature, exhibits also a dissolution enhancement effect. These results form a solid basis for the design and analysis of the aqueous mineral carbonation process. Particularly those in the presence of CO_2 indicate that aqueous carbonation requires a very delicate balancing between conditions favouring dissolution and those favouring precipitation based on a precise control of pH. Combining our results with those of thorough studies of magnesite precipitation could bring important new insights into our understanding of the entire mineral carbonation process.

Acknowledgments

Financial support from the Fondation Claude and Giuliana, Basel, Switzerland, is gratefully acknowledged.

Associate editor: Eric H. Oelkers

References

Awad, A., van Groos, A.F.K., Guggenheim, S., 2000. Forsteritic olivine: effect of crystallographic direction on dissolution kinetics. *Geochim. Cosmochim. Acta* **64**, 1765–1772.

Blum, A., Lasaga, A., 1988. Role of surface speciation in the low-temperature dissolution of minerals. *Nature* **331**, 431–433.

Brady, P.V., Dorn, R.I., Brazel, A.J., Clark, J., Moore, R.B., Glidewell, T., 1999. Direct measurement of the combined effects of lichen, rainfall, and temperature on silicate weathering. *Geochim. Cosmochim. Acta* **63**, 3293–3300.

Brantley, S.L., Mellott, N.P., 2000. Surface area and porosity of primary silicate minerals. *Am. Miner.* **85**, 1767–1783.

Chen, Y., Brantley, S.L., 2000. Dissolution of forsteritic olivine at 65 °C and 2 < pH < 5. *Chem. Geol.* **165**, 267–281.

Furrer, G., Stumm, W., 1986. The coordination chemistry of weathering: 1. Dissolution kinetics of Delta-Al_2O_3 and BeO. *Geochim. Cosmochim. Acta* **50**, 1847–1860.

Gautier, J.M., Oelkers, E.H., Schott, J., 2001. Are quartz dissolution rates proportional to BET surface areas? *Geochim. Cosmochim. Acta* **65**, 1059–1070.

Golubev, S.V., Pokrovsky, O.S., Schott, J., 2005. Experimental determination of the effect of dissolved CO_2 on the dissolution kinetics of Mg and Ca silicates at 25 °C. *Chem. Geol.* **217**, 227–238.

Grandstaff, D., 1986. The dissolution rate of forsteritic olivine from Hawaiian beach sand. In: Colman, S., Dethier, D. (Eds.), *Rates of Chemical Weathering of Rocks and Minerals*. Academic Press Inc., pp. 41–59.

Grasshoff, K., Anderson, L.G., 1999. *Methods of Seawater Analysis*, third ed. Wiley-VCH, Weinheim.

IPCC, 2005. IPCC special report on carbon dioxide capture and storage. Cambridge University Press, Cambridge, New York.

Jonckbloedt, R.C.L., 1998. Olivine dissolution in sulphuric acid at elevated temperatures—implications for the olivine process, an alternative waste acid neutralizing process. *J. Geochem. Explor.* **62**, 337–346.

Kump, L.R., Brantley, S.L., Arthur, M.A., 2000. Chemical, weathering, atmospheric CO_2, and climate. *Annu. Rev. Earth Planet. Sci.* **28**, 611–667.

Lackner, K.S., Wendt, C.H., Butt, D.P., Joyce, E.L., Sharp, D.H., 1995. carbon-dioxide disposal in carbonate minerals. *Energy* **20**, 1153–1170.

O'Connor, W.K., Dahlin, C.L., Rush, G.E., Gerdemann, S.J., Penner, L.R., Nilsen, D.N., 2004. Aqueous mineral carbonation: mineral availability, pretreatment, reaction parametrics, and process studies. Tech. Rep. DOE/ARC-TR-04-002, Albany Research Center.

Oelkers, E.H., 2001. An experimental study of forsterite dissolution rates as a function of temperature and aqueous Mg and Si concentrations. *Chem. Geol.* **175**, 485–494.

Park, A.H.A., Jadhav, R., Fan, L.S., 2003. CO_2 mineral sequestration: chemically enhanced aqueous carbonation of serpentine. *Can. J. Chem. Eng.* **81**, 885–890.

Pokrovsky, O.S., Schott, J., 2000. Kinetics and mechanism of forsterite dissolution at 25 °C and pH from 1 to 12. *Geochim. Cosmochim. Acta* **64**, 3313–3325.

Rosso, J.J., Rimstidt, J.D., 2000. A high resolution study of forsterite dissolution rates. *Geochim. Cosmochim. Acta* **64**, 797–811.

Van Herk, J., Pietersen, H.S., Schuiling, R.D., 1989. Neutralization of industrial-waste acids with olivine—the dissolution of forsteritic olivine at 40–70 °C. *Chem. Geol.* **76**, 341–352.

Wogelius, R.A., Walther, J.V., 1991. Olivine dissolution at 25 °C—effects of pH, CO_2, and organic-acids. *Geochim. Cosmochim. Acta* **55**, 943–954.

Wogelius, R.A., Walther, J.V., 1992. Olivine dissolution kinetics at near-surface conditions. *Chem. Geol.* **97**, 101–112.

Wolery, T.J. 1992. EQ3/6, a software package for geochemical modeling of aqueous systems: package overview and installation guide (Version 7.0). Tech. Rep. UCRL-MA-110662 PT I, Lawrence Livermore National Laboratory.

Wolf, G.H., Chizmeshya, A.V.G., Diefenbacher, J., McKelvy, M.J., 2004. In situ observation of CO_2 sequestration reactions using a novel microreaction system. *Environ. Sci. Technol.* **38**, 932–936.